Physicochemical and biological interactions between cerium oxide nanoparticles and a 1,8-naphthalimide derivative

Gerardo Pulido-Reyes, Esperanza Martín, J.L. Gu. Coronado, Francisco Leganes, Roberto Rosal, Francisca Fernández-Piñas, Physicochemical and biological interactions between cerium oxide nanoparticles and a 1,8-naphthalimide derivative, Journal of Photochemistry and Photobiology B: Biology, Volume 172, July 2017, Pages 61-69, ISSN 1011-1344, https://doi.org/10.1016/j.jphotobiol.2017.05.009.

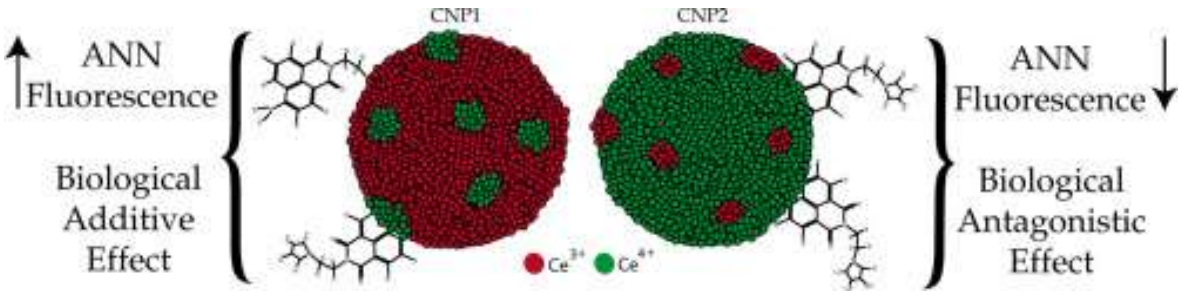

Physicochemical and biological interactions between cerium oxide nanoparticles and a 1,8-naphthalimide derivative

Gerardo Pulido-Reyesa[1,3,*], Esperanza Martín[2], J.L. Gu. Coronado[2], Francisco Leganes[1], Roberto Rosal[3], Francisca Fernández-Piñas[1]

[1] Departamento de Biología, Facultad de Ciencias, Universidad Autónoma de Madrid, E-28049, Spain

[2] Departamento de Química-Física Aplicada, Facultad de Ciencias, Universidad Autónoma de Madrid, E-28049, Spain

[3] Departamento de Ingeniería Química, Universidad de Alcalá, E-28871 Alcalá de Henares, Madrid, Spain

* Corresponding author: gerardo.pulido@uam.es

Abstract

Cerium (Ce) oxide nanoparticles (CNPs) have attracted attention due to their high bioactivity and unique redox-chemistry. The oxygen vacancies at the surface of the nanoparticle explain the autocatalytic properties of CNPs in which the Ce^{3+} atoms occupy the center of the oxygen vacancies surrounded by Ce^{4+} atoms. Until now, CNPs have been associated with organic molecules at the synthesis stage to extend their applications or improve their stability. However, there is a lack of information regarding the post-synthesis interaction of CNPs and organic molecules that could enhance or induce new properties. Due to their unique optical properties and their many uses in different areas such as supramolecular chemistry or biomedicine, we have chosen a derivative from the family of naphthalimides (the 4-amino-1,8-naphthalimide-N-substituted; ANN) to study the interaction with different CNPs (CNP1-4) and their joint bioactivity compared to that of the same compounds alone. ANN-CNP complexes were formed as revealed by spectroscopic studies, but, the interaction was markedly different depending on the physicochemical properties of CNPs and their surface content of Ce^{3+} sites. The ANN adsorption on all CNPs involved the amino group in the naphthalene moiety as shown by NMR spectroscopy, while the pyrrolidine ring was mainly involved in the specific interaction between ANN and CNP1. The biological effect of each CNP and ANN individually and forming complexes was assessed using a bioluminescent model bacterium. The results showed that ANN and CNP with the higher content of surface Ce^{3+} (CNP1) when combined acted additively towards the used model organism. In the opposite, ANN-CNP2, ANN-CNP3 and ANN-CNP4 complexes were antagonistic when the nanoparticles dominated the mixture. The results of this study contribute to expand the knowledge of the interaction between nanoparticles and organic molecules which may be useful for understanding the behavior of nanoparticles in complex matrices.

Keywords: Cerium oxide nanoparticles; 1,8-naphthalimide; Adsorption; Bioactivity; Mixture toxicity.

1. Introduction

Nowadays, nanoparticles of a huge diversity of materials, differing in their elemental composition, size, morphology and physical or chemical properties, can be synthesized through many different methods [1-3]. Cerium oxide nanoparticles are increasingly used in industrial applications such as glass polishing [4], solar cells [5] and fuel additives [6]. They have also been studied in biomedicine as anticancer agent [7-8] and oxidative stress scavenger [9-11], among others [12]. This variety of applications is derived from their high surface activity and unique redox-chemistry. The redox/catalytic properties of cerium oxide nanoparticles (CNPs) are a consequence of the existence of two possible surface oxidation states, Ce^{3+} and Ce^{4+}, which induce a redox couple [13]. In recent years, CNPs have been synthesized and functionalized with a variety of molecules such as small ligands [14], polymers [15-16], surfactants [17] and other organic molecules [18] using different strategies [19]. However, there are a lot of complex matrices (abiotic and biotic) where the surface of nanoparticles becomes adsorbs with external molecules that block the designed nanoparticle functionality [20-21].

Naphthalimides (1*H*-benzo[*de*]isoquinoline-1,3-(2*H*)-diones) represent a class of compounds widely used in a variety of fields [22-24]. Among other applications, naphthalimides have been used as dyes for synthetic fibers [25], optical brighteners in detergents and polymeric materials, solar energy collectors [26], ion sensors [27-29] and biomedicine as potential anti-cancer agents [30-31]. Chemically, 1,8-naphthalimide is a polar molecule with electron deficiency in the aromatic rings and an absorption band $n \rightarrow \pi^*$ type in the near-UV range. The introduction of substituents with electron donor character in 3- or 4-position of the naphthalene ring, such as amine ($-NH_2$) or methoxy ($-OCH_3$) group, generates a new band in the visible

frequency [32]. The absorption maximum of this band depends on the polarity of the solvent, due to the electronic $\pi \rightarrow \pi^*$ transition type has a charge transfer character towards the aromatic rings. It has been observed that the fluorescence quantum yield and fluorescence lifetime of these substituted compounds increase, especially in polar solvents such as acetonitrile and alcohols [23]. However, when the substituent in the imide nitrogen is an ethyl with a tertiary amino group, a fluorescence quenching is produced, a behavior associated to a Photo-induced Electron Transfer effect (PET) [33-34]. Thus, these singular spectroscopic properties of naphthalimide molecules make relatively easy to track their possible interaction with nanoparticles.

Nanoparticles in suspension may come in contact with organic pollutants [35] or biological molecules [36] giving rise to the formation of complexes which biological effect is starting to be fully studied. The combination may produce an effect greater than the sum of their individual effects (synergism) or lower (antagonism). In this work, we have used several CNPs and a 4-amine-N-[2-(1-pyrrolidin)ethyl]-1,8-naphthalimide (ANN, hereinafter) in order to investigate whether CNPs are capable of interacting with a 1,8-naphthalimide derivative by studying their spectroscopic properties and ANN-structural changes after the interaction with CNPs. We have also studied the biological effect of CNPs and ANN using a bioluminescent model bacterium.

2. Materials and Methods

2.1. Nanoparticle Synthesis and Characterization

Four Cerium Oxide Nanoparticles (CNPs) were synthesized using different methods with different surface Ce^{3+} contents and morphology. The physicochemical properties of the four nanoparticles were thoroughly analyzed. In particular, morphology and nominal size were assessed by High Resolution Transmission Electron Microscopy (HRTEM; FEI Tecnai F30). Ce^{3+}/Ce^{4+} ratios on the surface of nanoparticles were analyzed using X-Ray photoelectron spectroscopy (XPS) as described elsewhere (Deshpande, 2005). Hydrodynamic diameter and ζ-potential of the CNP suspensions in the different assay conditions were measured by Dynamic light scattering (DLS) and electrophoretic light scattering respectively using a Zetasizer Nano ZS particle size analyzer (Malvern Instruments Ltd.; Worcestershire, UK). Further details are given elsewhere [37].

2.2. Synthesis and Spectroscopic Properties of 4-amine-N-[2-(1-pyrrolidin)Ethyl]-1,8-naphthalimide

4-amine-N-[2-(1-pyrrolidin)ethyl]-1,8-naphthalimide (ANN) was synthesized according to a procedure described elsewhere [30]. Briefly, the ANN were synthesized by condensation between 4-amino-1,8-naphthalic anhydride and the 1-(2-aminoethyl) pyrrolidine. The absorption spectra were recorded in a double bean Perkin-Elmer Lambda 16 spectrophotometer (Perkin-Elmer, Massachusetts, USA). The fluorescence intensity was measured in a Schoeffel model 970 fluorimeter (Schoeffel Instrument Corp., New Jersey, USA). Fluorescence quantum yields were obtained using Norharmane solution (Sigma-Aldrich) in 0.1 N sulfuric acid as standard [38]. Fluorescence lifetime measurements were performed by using time-correlated single photon counting (TCSPC) spectroscopy with a hydrogen-filled flash as the excitation source (FWHM = 1 ns). The lifetimes were estimated from the measured fluorescence decay curves and the lamp profiles using a nonlinear least-squares iterative fitting procedure [39]. The quality of the fit was assessed by plotting the standard deviation and the chi-square values. All measurements were conducted at 10^{-5} M in three different solvents: dH_2O (pH 7), dichloromethane (DCM) and NaOH 0.01 M (pH 11). Fourier Transform InfraRed (FT-IR) spectra were obtained in KBr (1 wt%) using a Bruker model IFs 66 V Fourier Transform Infrared spectrometer in transmission mode.

2.3. Studying the ANN-CNPs Complex

The hydrodynamic diameter and ζ-potential of 10 mg/l CNP suspensions in 2.5 μM ANN in dH_2O, pH 7 were measured by Dynamic light scattering (DLS) and electrophoretic light scattering, respectively, using a Zetasizer Nano ZS particle size analyzer. The effect of the different CNPs on the absorption spectrum of ANN was measured using a Hitachi U-2000 spectrophotometer (Japan). Increasing concentrations of CNPs (8.6, 17.2, 172 mg/l) were used in order to track changes in the absorption spectrum. For it, the fluorescence emission at 560 nm of ANN with or without the presence of CNPs was analyzed during 30 min. Fluorescence readings were also taken every 10 min with a Synergy HT multi-mode microplate reader (BioTek, USA). The excitation wavelength was 360 nm.

^{1}H NMR spectra were obtained using 500 MHz Bruker Advance DRX Spectrometer equipped with a 5 mm BBOFplus 1H-19F/X *Z*-Grad and referenced to tetramethylsilane. The peak at 5.36 ppm and 4.80 ppm were related with dichloromethane (DCM) or water, respectively. Reference ANN spectrum was obtained in DCM. 10 μL of CNPs (6 mg/l; final concentration) was added to the naphthalimide derivative (0.1 mM) and the corresponding spectra were recorded after 30 min of incubation. The spectra were processed using MestreNova software (version 10.0.2–15,465).

2.4. Biological Assays

As a representative biological assay, we used a high-throughput configuration of a bioluminescent whole-cell biosensor that detects metabolic toxicity based on a bacterium (*Anabaena sp.* PCC7120 CPB4337;

hereinafter *A.* CPB4337) which has been used in several studies [40-41]. *A.* CPB4337 bears in the chromosome a Tn5 derivative with *luxCDABE* from the luminescent terrestrial bacterium *Photorhabdus luminescens*. This strain shows a high constitutive self-luminescence, so the bioassays are based on the inhibition of constitutive luminescence caused by the presence of a toxic substance. *A.* CPB4337 was also chosen because it has been previously shown that it cannot internalize cerium oxide nanoparticles [42]. Accordingly, the possible effects derived from internalized particles can be excluded. The dose-response curves of ANN and all CNPs were determined after 24 h of exposure in AA/8 medium supplemented with 5 mM nitrate (AA/8 + N; the composition of the bacterial growth medium is given in Supplementary table S1). The final concentrations tested ranged from 0 (control samples) to 75 μM (for ANN) or 75 mg/l (for each CNP). The No-Observed-Effect-Concentration (NOEC) and EC_{10} (the effective concentration of ANN or CNP that caused 10% bioluminescence inhibition with respect to a non-treated control) were obtained from the dose-response curves.

The bioassays were conducted in transparent sterile 24-well plates. Each well was filled with ANN, the nanoparticle suspension or the ANN-CNP combination at different ratios based on their NOECs and EC_{10}s. Three ratios were chosen for each: ANN_{NOEC}-CNP_{NOEC} (0.75:0.25; 0.5:0.5 and 0.25:0.75) and ANN_{EC10}-CNP_{EC10} (0.75:0.25; 0.5:0.5 and 0.25:0.75). After 30 min, AA/8 + N medium and *A.* CPB4337 were added to the wells to reach a final OD_{750nm} = 0.5. The 24-well plates were kept at 28 °C and light ca. 65 μmol photons m^2 s^{-1} on a rotary shaker during 24 h of exposure. For luminescence measurements, 100 ml of each sample were transferred to an opaque white 96-well plate and recorded in a Centro LB 960 luminometer for 10 min.

2.5. Statistics

Statistical analyses were performed by using R software 3.0.2. Measurements were analyzed essentially as described elsewhere [37]. At least three independent experiments with triplicate samples were performed. A one-way ANOVA coupled with Tukey's HSD (honestly significant difference) post-hoc test was performed for comparison of means. Differences were considered statistically significant when $p < 0.05$.

3. Results and Discussion

3.1. Photophysical Properties of N-substituted 1,8-naphthalimide

Fig. 1A shows the structure of the 4-amine-N-[2-(1-pyrrolidin)ethyl]-1,8-naphthalimide (ANN) used in this study. The molecule has an amino group in the 4-position of the naphthalene moiety and an aliphatic chain linked to the pyrrolidine ring by the imide group. Fig. 1B also shows the FT-IR spectrum of ANN in which the most characteristic bands were the carbonyl bands. Asymmetric and symmetric stretching vibration bands of the carbonyl groups of ANN appear in the 1680–1640 cm^{-1} range (the full FTIR transmission spectrum from 3600 to 1250 cm^{-1} can be found in Supplementary Fig. S1). The C—C stretching vibration bands of naphthalimide appeared in the 1620–1550 cm^{-1}region, while the C—N stretching vibration bands in the dicarboximide appeared between 1400 and 1350 cm^{-1}. In the 3100–3000 cm^{-1} region, typical C—H stretching vibration bands of aromatic rings were observed. The region around 3350 cm^{-1}corresponds to the stretching vibration of the N—H group. The C—H asymmetric and symmetric stretching vibration bands of the methylene groups of N-substituents laid in the 3000–2850 cm^{-1} region. These assignments are all in agreement with those results published by Grzesiak and Brycki [43] and Philipova [44] who did a deep FTIR analysis of some derivative of N-substituted-1,8-naphtalimides.

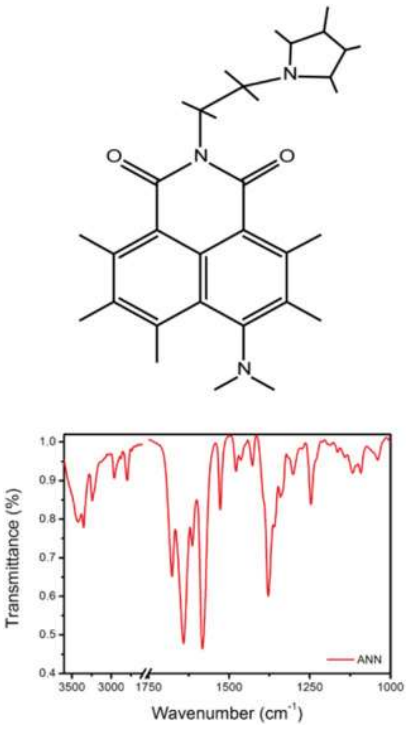

Figure 1. (A) Molecular structure of ANN. (B) FTIR transmission spectrum of ANN in the 3600–2600 and 1750–1000 cm−1 regions. A break at 1750 cm−1 was used to improve the clearness of the figure. The entire FTIR spectrum can be found in Supplementary Fig. S2.

The observed spectroscopic properties of ANN, namely absorption and fluorescence spectrum, quantum yield and fluorescence lifetime are presented in Table 1. The spectroscopic properties of ANN were pH and solvent polarity dependent: when ANN was diluted in DCM, there was a blue-shift from 433 nm to 407 nm in the absorption maximum and the fluorescence maximum changed to lower wavelength in comparison with the results obtained in NaOH 0.01 M and dH_2O (the complete absorption and emission spectra of ANN in dH_2O can be found in Supplementary Fig. S2). The

fluorescence quantum yields and lifetime of ANN also showed this dependence. ANN showed higher quantum yields in DCM than in dH_2O (Table 1). However, in NaOH solution, the fluorescence emission of ANN was strongly quenched by partial deprotonation of the amino group. The fluorescence lifetime showed that ANN in the organic solvent had the highest stabilization in the excited state. It is known that the 4-amino-1,8-naphthalimide derivatives are highly emissive in organic solvents such as DCM and chloroform, while significant quenching is observed in water [45]. Nevertheless, the use of 4-amino-naphthalimide as detection probe in water is well established and several 1,8-naphthalimide derivatives have been used for the sensing of different cations [46-47] and anions [33]. In these cases, upon interaction with proper chemicals, the changes may affect emission alone or both absorption and emission spectra.

Table 1. Spectral data of 4-amino-1,8-naphthalimide N-substituted (ANN) in distilled water, dichloromethane and sodium hydroxide (0.01 M).

Solvent	λ_{abs} (nm)	λ_{fluo} (nm)	Φ_F	τ_{flu} (ns)
dH_2O	433	536	0.055	2.82
DCM*	407	490	0.174	11.4
NaOH	430	543	$1.5 \cdot 10^{-6}$	4.8

* DCM = dichloromethane

3.2. Physicochemical Characterization of CNPs

According to HRTEM, CNP1 and CNP2 were spheres with diameters of approximately 6, and 9 nm, respectively. CNP3 had rod shape (325 nm long with a width of 22 nm) and CNP4 had cubic shape with a particle size around 50 nm. From the deconvolution of Ce (3d) XPS spectra, we determined that CNP1 had the highest amount of surface Ce^{3+}(58%) followed by CNP3 (36%), CNP2 (28%) and CNP4 (26%). Table 2 shows the physicochemical characteristics of the four CNPs at 10 mg/l suspended in dH_2O. Measured ζ-potential values (pH 7) of all CNPs showed that they were all positive, but CNP1 (0.57 ± 0.66 mV) had the lowest value in comparison with the other tested CNPs. According to DLS measurements, the effective diameters were in the 70–343 nm range (Table 2).

3.3. Characterization of the Interaction Between ANN and CNPs

Several experiments were conducted in order to verify the interaction of ANN with cerium oxide nanoparticles. For it, we obtained absorption spectra and stationary fluorescence maxima of the ANN-CNPs water mixtures. As shown in Fig. 2, ANN displayed an electronic interaction with CNP1, proved by the decrease in the absorption maximum at 433 nm of ANN for increasing concentrations of CNPs from 8.6 to 172 mg/l (Fig. 2A). A completely different behavior was observed for CNP2, CNP3 and CNP4 (Fig. 2B, C and D, respectively) as all of them caused a light dispersion effect and the disappearance of the absorption maxima of the naphthalimide molecule. We have also recorded the whole spectrum of CNPs to prove the absence of absorption peaks due to the nanoparticles in the same region (see Supplementary Fig. S3).

Table 2. Physicochemical properties of the tested Cerium Oxide Nanoparticles (CNPs) alone and mixed with ANN 2.5 μM in dH2O (pH 7).

Sample Name	Morphology	ζ-potential (mV)	Effective Diameter (nm)
CNP1	Spheres	0.57 ± 0.66	70.2
CNP2	Spheres	12.0 ± 0.99	342.1
CNP3	Rods	15.9 ± 0.45	122.4
CNP4	Cubes	30.2 ± 0.66	190.1
			2.5 μM ANN
		ζ-potential (mV)	Effective Diameter (nm)
CNP1		-0.26 ± 0.66	200.2
CNP2		5.76 ± 0.26	458.7
CNP3		15.0 ± 0.66	220.2
CNP4		26.3 ± 0.21	255.2

Moreover, fluorescence spectroscopy was conducted to follow changes in the fluorescence behavior of ANN derived of the exposure with CNPs. Fig. 3 shows the fluorescence emission maximum at 530 nm of ANN and ANN-mixtures with CNP1, CNP2, CNP3 and CNP4 after 30 min of contact. CNP1 statistically ($p < 0.05$) increased the fluorescence emission of ANN by 6.7% when compared to the ANN alone. Conversely, CNP2, CNP3 and CNP4 statistically ($p < 0.05$) decreased the fluorescence emission maxima of ANN by 7.6, 7.9 and 9.6%, respectively. We also tracked the fluorescence variation over time, but the same pattern was observed (Supplementary Fig. S4).

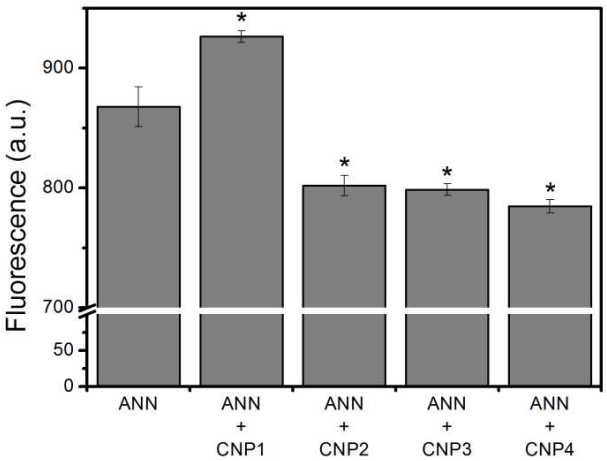

Figure 3. Fluorescence emission of ANN and mixtures between ANN and CNP1, CNP2, CNP3 and CNP4 at 560 nm (the excitation wavelength was 360 nm). Statistically significant differences ($p < 0.05$) are marked by asterisks.

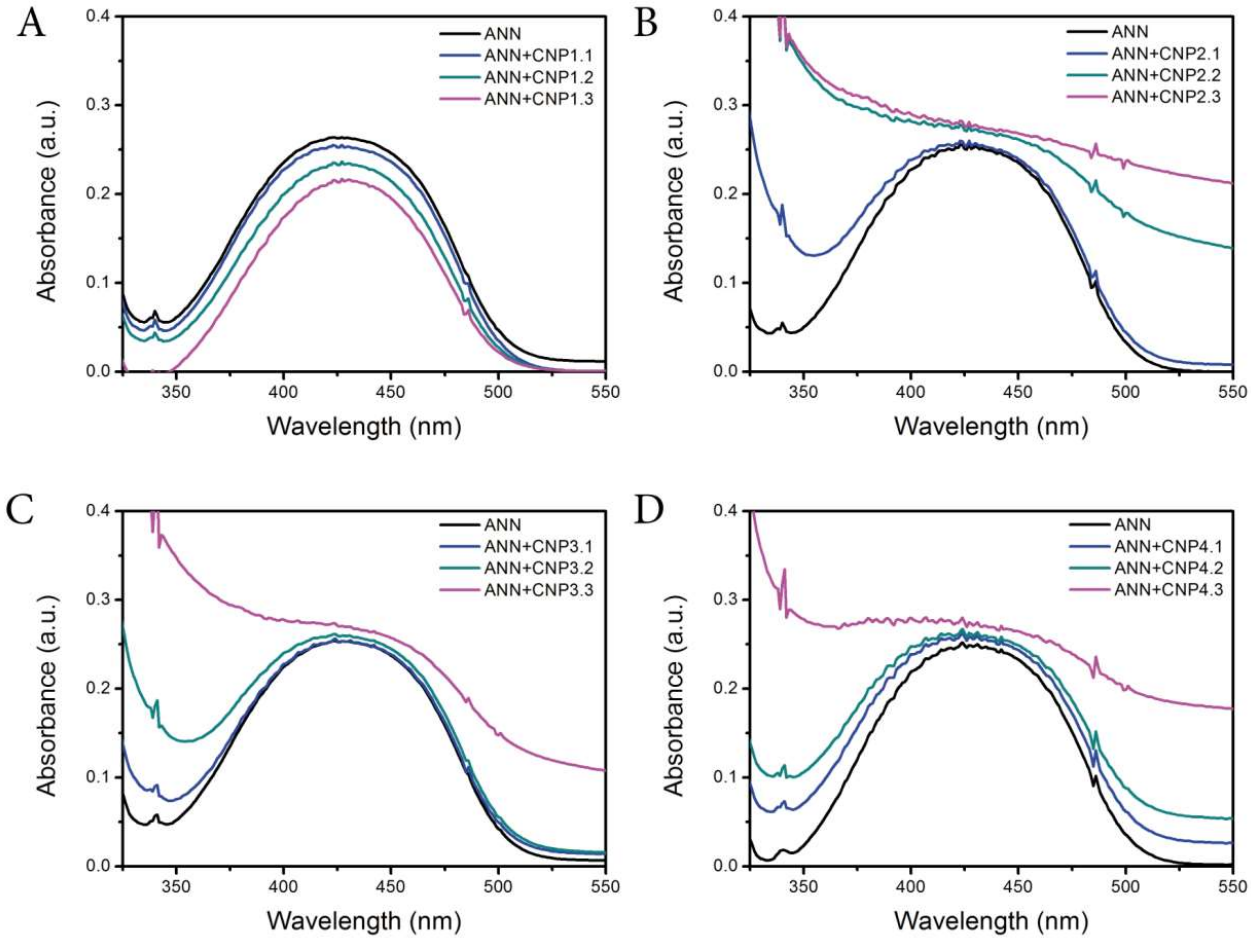

Figure 2. Changes in the UV-vis spectra of ANN 0.2 mM in the presence of increasing concentration of CNPs in dH_2O. CNPs concentrations were 8.6 (CNPx.1), 17.2 (CNPx.2) and 172 mg/l (CNPx.3).

The physicochemical properties of the nanoparticles also change upon contact with ANN. ANN increased the hydrodynamic size of all CNPs, with a particularly relevant increase for CNP1 (from 70 to 200 nm; Table 2). Moreover, the ζ-potential of all CNPs slightly decreased when ANN was added, denoting lower stability of CNPs. Therefore, the increment in the nanoparticle hydrodynamic size suggests that ANN interacts with all the CNPs, but the higher aggregation of CNP1 after contact with ANN is probably a consequence of a preferential interaction with ANN.

We used NMR spectroscopy for determining the structural changes of the organic compound after interaction with CNPs. Fig. 4 shows the NMR spectra of ANN and ANN-CNPs. The peaks of hydrogens in the naphthalene ring (from 8.7 to 6.7 ppm) and the primary amino group in 4-position (5.19 ppm) exhibited a left shift for all ANN-CNP complexes in comparison with the spectrum of ANN alone. This is indicative of a lower electronic density in this region (lower shielding of these hydrogens) due to the interaction with CNPs. There were no significant changes in other regions of the spectra.

Taking all these results together, we determined that ANN is able to adsorb onto the surface of CNPs. In view of NMR results, it is reasonable that all CNPs adsorb ANN through the naphthalene ring and the primary amino group. However, the main advantages of using ANN is that it has an internal charge transfer in the excited state, due to the electron donating amine and the electron withdrawing tertiary amine pyrrolidine group (PET) [33, 48]. This particularity could also be considered for determining how ANN interacts with the surface of nanoparticles. Accordingly, the formation of an ANN-CNP1 complex leading to the increment of the ANN-fluorescence (Fig. 3) suggests an interaction through the pyrrolidine ring and the aliphatic chain, because the PET process in this case would be inhibited by CNP1. The smallest nominal size along with the sphere morphology of CNP1 could also favor the interaction on this region of the molecule. It has been previously shown that the pyrrolidine ring of several 1,8-naphthalimide N-substituted molecules could fold to the molecular plane in certain circumstances, preventing the interaction in this region with nanoparticle with higher sizes and different morphologies [34]. Conversely, CNP2, CNP3 and CNP4 would strongly interact with the primary amino moiety of ANN, enhancing PET process and, thus, reducing the fluorescence of the chromophore as shown in Fig. 3 and in agreement with NMR data.

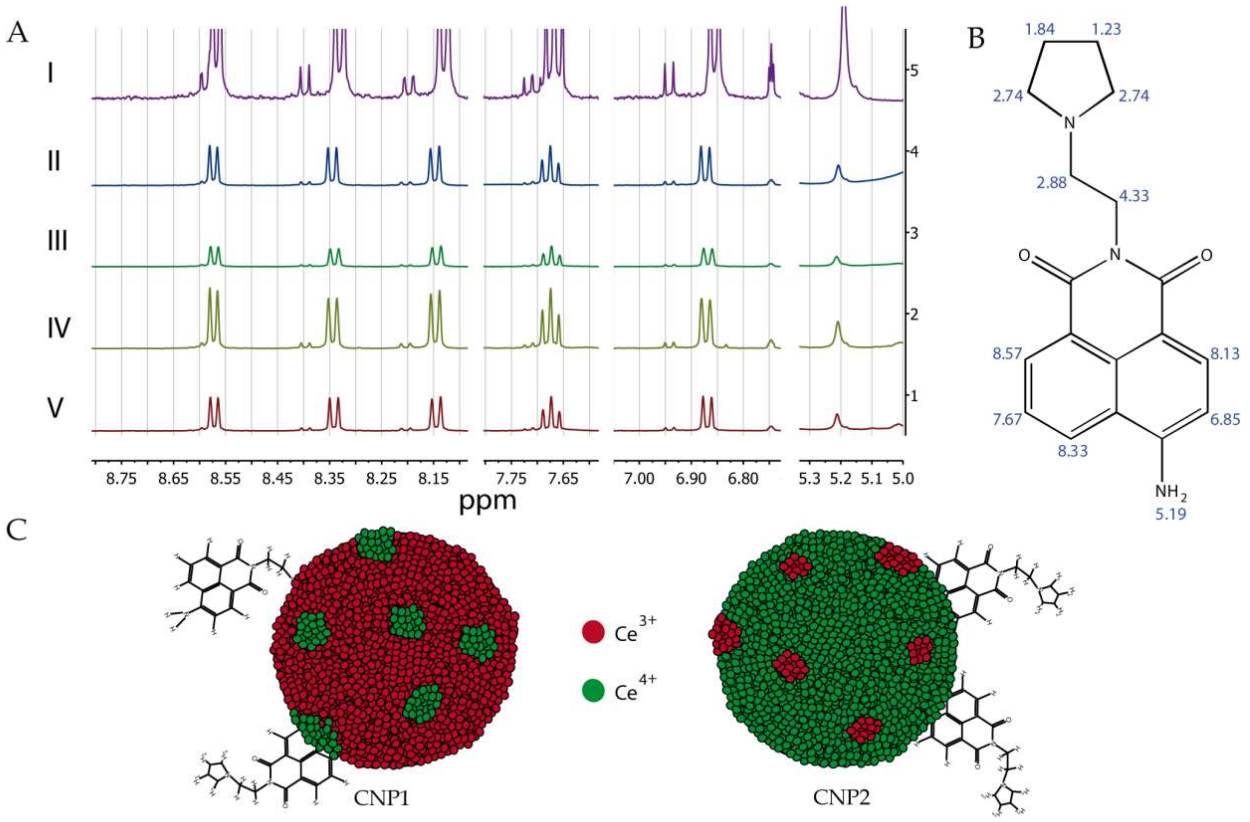

Figure 4. (A) Selected ^{1}H NMR spectra of compound ANN alone (I) or with CNP1 (II), CNP2 (III), CNP3 (IV) and CNP4 (V). (B) Molecular designation of each H in order to facilitate the description of RMN results. (C) Schematic representation of the adsorption of ANN on the CNP1 or CNP2 surface depending of the Ce^{3+}/Ce^{4+} sites (the sizes are not representative).

The nanoparticle surface chemistry may be responsible for the different interaction of ANN with CNPs. CNP2, CNP3 and CNP4 had a relatively low surface Ce^{3+} content (between 26 and 36%) and, therefore, their surface chemistry is governed by the Ce^{4+} form. CNP1, on the other hand, also has Ce^{4+} in its surface, but in a lower percentage. Upon ANN-CNP interaction, the surface Ce^{4+} can be reduced by the unpaired electron of the amine nitrogen as the redox potential of ANN is −1.92 V [32]. The ANN molecule has a tendency to lose electrons which could stabilize the complex formed with CNPs. Fig. 4C illustrates how ANN interacts with CNP1 through the pyrrolidine ring and naphthalene moiety, while only the amino moiety was involved during the interaction between ANN and CNP2, CNP3 and CNP4 (CNP1 and CNP2 were chosen in Fig. 4C to show this hypothesis).

Other factors than % surface Ce^{3+} may influence the adsorption of ANN on CNPs, such as surface facet and oxygen vacancies, but it is not clear which one is responsible for the reactivity of CNPs under a given set of conditions. Recently, Yang et al. [49] suggested that the facets of CNPs are more relevant for explaining redox activity than the % surface Ce^{3+}. In support for this hypothesis, particles with {100} facets displayed higher catalytic activity than particles with other facets but similar levels of surface Ce^{3+}. However, other authors argued that several factors would be required to explain the reactivity of CNPs. In fact, particles with higher amount of the most reactive facet towards photocatalytic oxidation of volatile organics were less effective in the photocatalytic O_2 evolution, indicating that the surface facet itself could not fully explain the observed catalytic behavior [50]. The particles used in this work exposed different surface facet terminations. According to the existing literature, ceria nanocubes and nanorods are dominantly terminated by {100} and {110} + {100} facets, respectively [50-52]. Conversely, sphere-like CNPs expose {100} truncated {111} octahedron [53]. The similar mode of interaction found for CNP2, CNP3 and CNP4, which have different facets, with ANN suggested that the % surface of Ce^{3+} was more relevant than the surface facet composition for the interaction of ANN and CNP. Moreover, the predominance of facets on the reactivity of CNPs proposed by Yang et al. [49] may be appropriate for enzymatic-mimetic reactions as they have demonstrated, but it could not be suitable for photochemical interactions such as those described here in the formation of ANN-CNP complexes.

3.4. Biological Effect of ANN, CNPs and ANN-CNP Towards *Anabaena* CPB4337

The concentration-response curve for 24 h luminescence inhibition is shown in Fig. 5 for ANN and

the four CNPs over the whole concentration range studied. While ANN and CNP1 caused a 100% bioluminescence inhibition at 50 μM and 30 mg/l, respectively; CNP2, CNP3 and CNP4 were non-toxic, with EC_{20} near the maximum concentration tested in this work (75 mg/l). Additionally, from these dose-response curves, we have calculated the NOEC and the sublethal EC_{10} of each compound, which were used as reference levels during the assessment of the biological effect of the ANN-CNP complexes (Fig. 6). Those concentrations are relatively low, but chosen in purpose, in order to design experiments which may be closer to real world scenarios. In biomedicine, it is necessary to use efficient concentration to avoid negative collateral effects. For concentrations higher than 75 mg/l, CNP1, for example, was very toxic, thus cells would have been severely damaged or even dead and it would have not been possible to study the biological effects. Different ratios were chosen in order to evaluate the possible additive, antagonistic or synergistic effect of the ANN-CNP complexes. As shown in Fig. 6A, when ANN and CNP were mixed at the NOEC level, there were no statistical effects at any ANN-CNP ratio in comparison with ANN or CNP alone. Nevertheless, a different effect was observed when ANN and CNP were mixed at the EC_{10} level. The 0.25:0.75 ratio of ANN-CNP2, ANN-CNP3 and ANN-CNP4 statistically ($p < 0.05$) reduced the expected adverse effect (antagonism): the luminescence inhibition of these samples was less than the sum of the known effects of the individual substances. This effect was not observed for the other ratios (0.5:0.5 and 0.75:0.25) or ANN-CNP1 complex whose mixture showed an additive effect. As mentioned before, it has been shown that CNPs have several mimetic antioxidant properties derived from their surface redox chemistry. The adsorption of ANN onto the surface of these nanoparticles could enhance these properties for CNP2, CNP3 and CNP4 (nanoparticles with low surface % of Ce^{3+}), which would also explain lower effect of 0.25:0.75 mixtures at the EC_{10} level. In fact, at the NOEC level, a slight luminescence stimulation was observed.

The bioluminescent model bacterium *A.* CPB4337 is a quantitative high-throughput screening (QHTS) method described previously [40]. The use of this organism generates fast and accurate information about the biological effect of different compounds in a short period of time. As the bacterium used here is very different from a mammalian cell, *A.* CPB4337 could be probably more resistant, due to the cell wall envelope which covers the cell. However, several test based on bacteria (Ames test [54] and *Vibrio fischeri* test [55]) have been used as first approximation of the biological effect of toxicants and it is well stablished their use in the risk management and health and safety assessment of substances.

It has been previously described that naphthalimide derivatives can enter inside different cell types [56] and depending on the derivative and their substituents, it

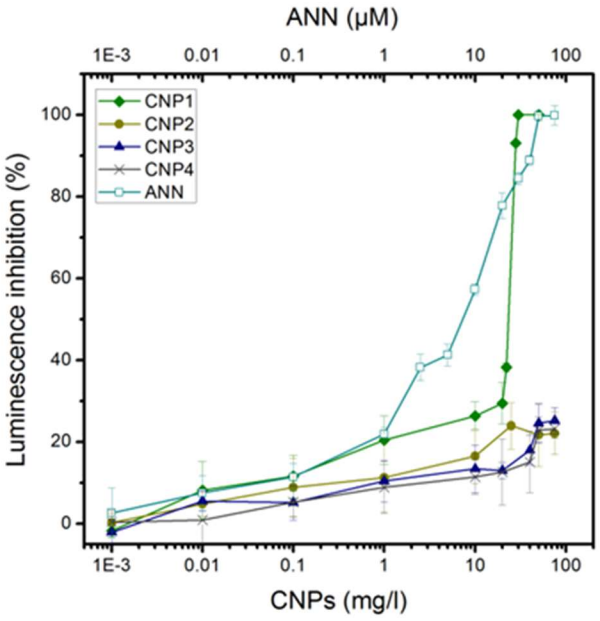

Figure 5. Dose-response curve of ANN (from 0.001 to 100 μM), CNP1, CNP2, CNP3 and CNP4 (nanoparticle concentrations from 0.001 to 100 mg/l) for *Anabaena* CPB4337. At least three independent experiments with three replicates were used (n = 9).

has been evidenced that some could interact with nucleic acids by intercalation [57] and others may directly break the cellular membrane [58], exerting their toxic effect in mammalian and bacterial cells, respectively. Although the ANN mode of action is beyond the aims of this study, we consider that the negative biological effect could be mediated both by direct membrane interaction (due to the non-polar nature of the molecule) and by intracellular impact on nucleic acid. We did not observe any CNP internalization in our previous study using *A.* CPB4337 and ceria-based nanoparticles [42], so this organism was chosen to avoid the possible effects derived from internalized particles. The direct contact between cell envelope and nanoparticles, resulting in cell wall and membrane disruption and cell lysis, was proposed as the mechanism underlying CNP toxicity. Moreover, the hydrodynamic size of ANN-CNPs complex is higher than the diameter of 20 nm suggested for the pores of envelope of *Anabaena* sp. PCC 7120 [59], and therefore neither CNP alone or CNP-formed complex could be internalized. The observed antagonistic effect for ANN-CNP2, ANN-CNP3 and ANN-CNP4 could be due to several causes: On the one hand, the formation of the ANN-CNP complex could reduce the bioavailability of ANN avoiding its entry into the cells and the production of its toxic effect. On the other hand, the ANN-CNP complex could also interfere in the interaction between CNP and the cell wall, as it has been shown that the formation of a corona on the surface of nanoparticles could reduce the observed toxicity of the nanoparticle alone [60].

The aggregation of CNPs and CNPs forming complexes with ANN was clear as stated in Table 2. However, the

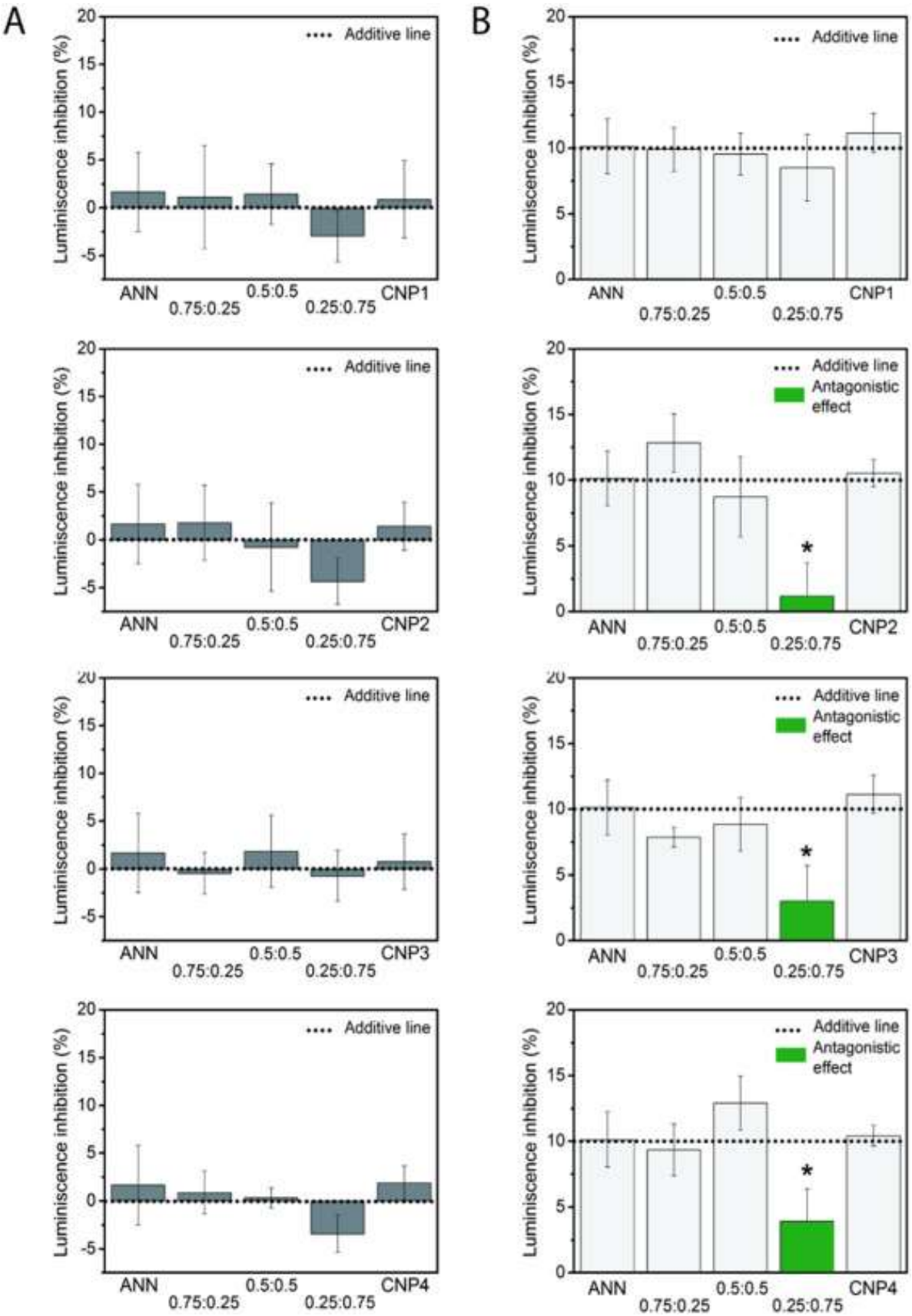

Figure 6. Bioluminescence Inhibition of *A.* CPB4337 in response to ANN-CNPs complexes after 24 h. A) Effect of the ANN-CNPs complex using different ratios at the No-Observed-Effect-Concentration (NOEC). B) Effect of the ANN-CNPs complexes using different ratios at the effective concentration of ANN or CNPs that caused 10% bioluminescence inhibition with respect to a non-treated control (EC_{10}). The green bars indicate antagonism and the dotted line additivity. In all figures the response of *A.* CPB4337 to ANN and CNPs applied singly is also shown for comparison. Mean ± standard deviation. Statistically significant differences ($p < 0.05$) are marked by asterisks. (For interpretation of the references to colour in this figure legend, the reader is referred to the web version of this article.)

formation of aggregates did not influence the adsorption of ANN on the surface of CNP. It could be argued that the lower degree of aggregation of CNP1 could favor the interaction with ANN due to its higher surface to volume ratio in comparison with the other CNPs. However, this different aggregation degree did not have a relevant effect on the biological experiments with the tested model organism, since ANN-CNP2, ANN-CNP3 and ANN-CNP4, which formed the largest aggregates, showed protective/antagonistic effect. In a previous publication, several factors were evaluated as possible drivers of the toxicity of various cerium oxide nanoparticles, including size/surface aggregation [37]. Among them, the % surface Ce^{3+} was the dominant factor as demonstrated by the fact that phosphate blocked Ce^{3+} sites and totally reverted the toxicity of CNP with the highest % surface Ce^{3+}, as a consequence of the affinity of surface Ce^{3+} to phosphate.

To the best of our knowledge, there were found no articles evaluating the toxicity of naphthalimide derivatives and only few articles studying their interaction with nanomaterials. Aguilera-Sigalat et al. [61] synthesized quantum dots (QDs) capped with ligands that possess a naphthalimide as chromophore unit with the objective of controlling the emission properties of CdSe/ZnS QDs through naphthalimide derivatives [61]. Moreover, dendrimers with amino-1,8-naphthalimide molecules in their structures were proposed as tunable organic light-emitting diodes [62]. Bekere et al. [63] evaluated the possibility of using 4-substituted 1,8-naphthalimides as sensitive molecular probes for ZnO nanoparticles. In this case, the nature of the interaction and how the molecule was adsorbed onto the nanoparticle were not studied. Huang et al. [64] showed that nanoparticle surface characteristics were key parameters during protein adsorption, since they might be able to modulate the protein conformation onto nanoparticle surface [64]. In this work, we showed that the surface Ce^{3+} content strongly affect the adsorption of 1,8-Naphthalimide onto CNPs. Furthermore, the fact that the ANN could increase its fluorescence emission in presence of CNP with high surface Ce^{3+} suggests their use of N-substituted 1,8-naphthalimides as specific selective probes to detect nanoparticles in water and in biological samples. In this respect, 1,8-naphthalimides are able to cross the cell membrane, so it would be possible to track nanoparticles inside the cells and show their exact location.

Nanotechnology is growing quickly, and it is expected that many products will have some kind of nanomaterial. The exponential increment of the number of potential applications is also probable. However, there is a lack of methodologies for the detection and characterization of engineered nanomaterials in complex matrices. It is necessary to develop new methods to solve this problem. In this regard, studies such as those provided by Othman et al. [65] and Chatterjee et al. [66] shed light on this issue when assessing the detection of nanoparticle by using specific organic dyes. Othman et al. (2016) described a method that was selectively optimized for the detection of CNP rather than any other metal oxide nanoparticles also in real water samples. In this regard, our results shown here provide a deeper insight on the interaction between an organic dye and nanoparticles, which could result in the direct detection of CNP in biological samples.

On the other hand, the use of combined molecules to fight against cancer is a standard clinical practice in the treatment of different tumors [67]. As stated above, several studies support the idea of using CNPs or 1,8-naphthalimide derivatives as anti-cancer agents. However, the biological results shown here reveal that, depending on the chosen CNP, their expected effect could be reduced if used in mixture.

4. Conclusions

In conclusion, in this work we demonstrated that cerium oxide nanoparticles can alter the spectroscopic properties of the 4-amine-N-[2-(1-pyrrolidin)ethyl]-1,8-naphthalimide and that the nanoparticle interaction with the organic molecule depends on their physicochemical characteristics. CNPs with high content of surface Ce^{3+} increased the fluorescence of ANN by interaction through the pyrrolidine ring; this complex caused an additive effect towards the bioluminescent model bacterium *A.* CPB4337. Conversely, CNPs with high content of surface Ce^{4+} decreased the ANN-fluorescence by enhancing PET process in the amino group and caused an antagonistic effect towards *A.* CPB4337. This study reveals a complex interaction between CNPs and 1,8-naphthalmide derivative which might cause an inefficiency use of these compounds even at low concentrations if they are used jointly as anticancer agents. The use of different mammalian and tumor cell lines will be needed to confirm the effects observed here. Besides, the results shown also contribute to untangle the unpredictable behavior of nanoparticles when they are suspended in complex matrices and open up a research line in the use of organic molecules to detect nanoparticle in liquid and biological samples.

Acknowledgements

This research was supported by CTM2013-45775-C2-1-R and CTM2013-45775-C2-2-R grants from MINECO. Cerium oxide nanoparticles were kindly provided by S. Seal and S. Das (University of Central Florida, U.S.A). Gerardo Pulido-Reyes thanks the Spanish Ministry of Education for the award of an FPU grant (FPU12/01796).

References

[1] M. Stefaniuk, P. Oleszczuk, Y.S. Ok. Review on nano zerovalent iron (nZVI): from synthesis to environmental applications. Chem. Eng. J., 287 (2016), pp. 618–632

[2] X. Chen, S.S. Mao. Titanium dioxide nanomaterials: synthesis, properties, modifications, and applications. Chem. Rev., 107 (2007), pp. 2891–2959
[3] A.H. Lu, E.L. Salabas, F. Schüth. Magnetic nanoparticles: synthesis, protection, functionalization, and application. Angew. Chem. Int. Ed., 46 (2007), pp. 1222–1244
[4] P.V. Dandu, B. Peethala, S. Babu. Role of different additives on silicon dioxide film removal rate during chemical mechanical polishing using ceria-based dispersions. J. Electrochem. Soc., 157 (2010), pp. H869–H874
[5] A. Corma, P. Atienzar, H. García, J.-Y. Chane-Ching. Hierarchically mesostructured doped CeO2 with potential for solar-cell use. Nat. Mater., 3 (2004), pp. 394–397
[6] D. Mei, X. Li, Q. Wu, P. Sun. Role of cerium oxide nanoparticles as diesel additives in combustion efficiency improvements and emission reduction. J. Energy Eng., 142 (2015), Article 04015050
[7] L. Alili, M. Sack, A.S. Karakoti, S. Teuber, K. Puschmann, S.M. Hirst, C.M. Reilly, K. Zanger, W. Stahl, S. Das. Combined cytotoxic and anti-invasive properties of redox-active nanoparticles in tumor–stroma interactions. Biomaterials, 32 (2011), pp. 2918–2929
[8] M.S. Wason, J. Colon, S. Das, S. Seal, J. Turkson, J. Zhao, C.H. Baker. Sensitization of pancreatic cancer cells to radiation by cerium oxide nanoparticle-induced ROS production. Nanomed.: Nanotechnol., Biol. Med., 9 (2013), pp. 558–569
[9] E.G. Heckert, A.S. Karakoti, S. Seal, W.T. Self. The role of cerium redox state in the SOD mimetic activity of nanoceria. Biomaterials, 29 (2008), pp. 2705–2709
[10] T. Pirmohamed, J.M. Dowding, S. Singh, B. Wasserman, E. Heckert, A.S. Karakoti, J.E. King, S. Seal, W.T. Self. Nanoceria exhibit redox state-dependent catalase mimetic activity. Chem. Commun., 46 (2010), pp. 2736–2738
[11] G. Pulido-Reyes, S. Das, F. Leganés, S. Silva, S. Wu, W. Self, F. Fernández-Piñas, R. Rosal, S. Seal. Hypochlorite scavenging activity of cerium oxide nanoparticles. RSC Adv., 6 (2016), pp. 62911–62915
[12] K. Reed, A. Cormack, A. Kulkarni, M. Mayton, D. Sayle, F. Klaessig, B. Stadler. Exploring the properties and applications of nanoceria: is there still plenty of room at the bottom? Environ. Sci.: Nano, 1 (2014), pp. 390–405
[13] F. Esch, S. Fabris, L. Zhou, T. Montini, C. Africh, P. Fornasiero, G. Comelli, R. Rosei. Electron localization determines defect formation on ceria substrates. Science, 309 (2005), pp. 752–755
[14] L. Qi, A. Sehgal, J.-C. Castaing, J.-P. Chapel, J. Fresnais, J.-F. Berret, F. Cousin. Redispersible hybrid nanopowders: cerium oxide nanoparticle complexes with phosphonated-PEG oligomers. ACS Nano, 2 (2008), pp. 879–888
[15] A. Asati, S. Santra, C. Kaittanis, S. Nath, J.M. Perez. Oxidase-like activity of polymer-coated cerium oxide nanoparticles. Angew. Chem., 48 (2009), pp. 2308–2312
[16] A.S. Karakoti, S. Singh, A. Kumar, M. Malinska, S.V. Kuchibhatla, K. Wozniak, W.T. Self, S. Seal. PEGylated nanoceria as radical scavenger with tunable redox chemistry. J. Am. Chem. Soc., 131 (2009), pp. 14144–14145
[17] Z. Wu, J. Zhang, R.E. Benfield, Y. Ding, D. Grandjean, Z. Zhang, X. Ju. Structure and chemical transformation in cerium oxide nanoparticles coated by surfactant cetyltrimethylammonium bromide (CTAB): an X-ray absorption spectroscopic study. J. Phys. Chem. B, 106 (2002), pp. 4569–4577
[18] M. Hijaz, S. Das, I. Mert, A. Gupta, Z. Al-Wahab, C. Tebbe, S. Dar, J. Chhina, S. Giri, A. Munkarah. Folic acid tagged nanoceria as a novel therapeutic agent in ovarian cancer. BMC Cancer, 16 (2016), p. 220
[19] S. Das, J.M. Dowding, K.E. Klump, J.F. McGinnis, W. Self, S. Seal. Cerium oxide nanoparticles: applications and prospects in nanomedicine. Nanomedicine (London), 8 (2013), pp. 1483–1508
[20] A. Salvati, A.S. Pitek, M.P. Monopoli, K. Prapainop, F.B. Bombelli, D.R. Hristov, P.M. Kelly, C. Åberg, E. Mahon, K.A. Dawson. Transferrin-functionalized nanoparticles lose their targeting capabilities when a biomolecule corona adsorbs on the surface. Nat. Nanotechnol., 8 (2013), pp. 137–143
[21] B.S. Varnamkhasti, H. Hosseinzadeh, M. Azhdarzadeh, S.Y. Vafaei, M. Esfandyari-Manesh, Z.H. Mirzaie, M. Amini, S.N. Ostad, F. Atyabi, R. Dinarvand. Protein corona hampers targeting potential of MUC1 aptamer functionalized SN-38 core–shell nanoparticles. Int. J. Pharm., 494 (2015), pp. 430–444
[22] Q. Xuhong, Z. Zhenghua, C. Kongchang. The synthesis, application and prediction of stokes shift in fluorescent dyes derived from 1, 8-naphthalic anhydride. Dyes Pigments, 11 (1989), pp. 13–20
[23] E. Martin, R. Weigand, A. Pardo. Solvent dependence of the inhibition of intramolecular charge-transfer in N-substituted 1, 8-naphthalimide derivatives as dye lasers. J. Lumin., 68 (1996), pp. 157–164
[24] S. Banerjee, E.B. Veale, C.M. Phelan, S.A. Murphy, G.M. Tocci, L.J. Gillespie, D.O. Frimannsson, J.M. Kelly, T. Gunnlaugsson. Recent advances in the development of 1, 8-naphthalimide based DNA targeting binders, anticancer and fluorescent cellular imaging agents. Chem. Soc. Rev., 42 (2013), pp. 1601–1618
[25] A. Peters, M. Bide. Amino derivatives of 1, 8-naphthalic anhydride and derived dyes for synthetic-polymer fibres. Dyes Pigments, 6 (1985), pp. 349–375
[26] G.R. Bardajee, A.Y. Li, J.C. Haley, M.A. Winnik. The synthesis and spectroscopic properties of novel, functional fluorescent naphthalimide dyes. Dyes Pigments, 79 (2008), pp. 24–32
[27] D. Cui, X. Qian, F. Liu, R. Zhang. Novel fluorescent pH sensors based on intramolecular hydrogen bonding ability of naphthalimide. Org. Lett., 6 (2004), pp. 2757–2760
[28] F.M. Pfeffer, A.M. Buschgens, N.W. Barnett, T. Gunnlaugsson, P.E. Kruger. 4-amino-1, 8-naphthalimide-based anion receptors: employing the naphthalimide N–H moiety in the cooperative binding of dihydrogenphosphate. Tetrahedron Lett., 46 (2005), pp. 6579–6584
[29] H.-H. Lin, Y.-C. Chan, J.-W. Chen, C.-C. Chang. Aggregation-induced emission enhancement characteristics of naphthalimide derivatives and their applications in cell imaging. J. Mater. Chem., 21 (2011), pp. 3170–3177

[30] M. Brana, J. Castellano, C. Roldan, A. Santos, D. Vazquez, A. Jimenez. Synthesis and mode (s) of action of a new series of imide derivatives of 3-nitro-1, 8 naphthalic acid. Cancer Chemother. Pharmacol., 4 (1980), pp. 61–66
[31] J. Noro, J. Maciel, D. Duarte, A. Olival, C. Baptista, A. Silva, M. Alves, P. Kong Thoo Lin. Evaluation of new Naphthalimides as Potential Anticancer Agents Against Breast Cancer MCF-7, Pancreatic Cancer BxPC-3 and Colon Cancer HCT-15 Cell Lines (2015)
[32] E. Martın, R. Weigand. A correlation between redox potentials and photophysical behaviour of compounds with intramolecular charge transfer: application to N-substituted 1, 8-naphthalimide derivatives. Chem. Phys. Lett., 288 (1998), pp. 52–58
[33] T. Gunnlaugsson, P.E. Kruger, T.C. Lee, R. Parkesh, F.M. Pfeffer, G.M. Hussey. Dual responsive chemosensors for anions: the combination of fluorescent PET (Photoinduced Electron Transfer) and colorimetric chemosensors in a single molecule. Tetrahedron Lett., 44 (2003), pp. 6575–6578
[34] E. Martín, J.L.G. Coronado, J.J. Camacho, A. Pardo. Experimental and theoretical study of the intramolecular charge transfer on the derivatives 4-methoxy and 4-acetamide 1,8-naphthalimide N-substituted. J. Photochem. Photobiol. A Chem., 175 (2005), pp. 1–7
[35] J.R. Lead, K.J. Wilkinson. Aquatic colloids and nanoparticles: current knowledge and future trends. Environ. Chem., 3 (2006), pp. 159–171
[36] I. Lynch, K.A. Dawson. Protein-nanoparticle interactions. Nano Today, 3 (2008), pp. 40–47
[37] G. Pulido-Reyes, I. Rodea-Palomares, S. Das, T.S. Sakthivel, F. Leganes, R. Rosal, S. Seal, F. Fernández-Piñas. Untangling the biological effects of cerium oxide nanoparticles: the role of surface valence states. Sci. Rep., 5 (2015), p. 15613
[38] A. Pardo, D. Reyman, J. Poyato, F. Medina. Some β-carboline derivatives as fluorescence standards. J. Lumin., 51 (1992), pp. 269–274
[39] D. O'Connor. Time-correlated Single Photon Counting. Academic Press (2012)
[40] I. Rodea-Palomares, M. Gonzalez-Pleiter, S. Gonzalo, R. Rosal, F. Leganes, S. Sabater, M. Casellas, R. Muñoz-Carpena, F. Fernández-Piñas. Hidden drivers of low-dose pharmaceutical pollutant mixtures revealed by the novel GSA-QHTS screening method. Sci. Adv., 2 (2016), Article e1601272
[41] M. González-Pleiter, S. Gonzalo, I. Rodea-Palomares, F. Leganés, R. Rosal, K. Boltes, E. Marco, F. Fernández-Piñas. Toxicity of five antibiotics and their mixtures towards photosynthetic aquatic organisms: implications for environmental risk assessment. Water Res., 47 (2013), pp. 2050–2064
[42] I. Rodea-Palomares, K. Boltes, F. Fernandez-Pinas, F. Leganes, E. Garcia-Calvo, J. Santiago, R. Rosal. Physicochemical characterization and ecotoxicological assessment of CeO2 nanoparticles using two aquatic microorganisms. Toxicol. Sci., 119 (2011), pp. 135–145
[43] W. Grzesiak, B. Brycki. Synthesis, FTIR, 13C-NMR and temperature-dependent 1H-NMR characteristics of Bis-naphthalimide derivatives. Molecules, 17 (2012), pp. 12427–12448
[44] T. Philipova, I. Karamancheva, I. Grabchev. Absorption spectra of some N-substituted-1, 8-naphthalimides. Dyes Pigments, 28 (1995), pp. 91–99
[45] X. Poteau, A.I. Brown, R.G. Brown, C. Holmes, D. Matthew. Fluorescence switching in 4-amino-1, 8-naphthalimides: “on–off–on” operation controlled by solvent and cations. Dyes Pigments, 47 (2000), pp. 91–105
[46] R. Parkesh, T.C. Lee, T. Gunnlaugsson. Highly selective 4-amino-1, 8-naphthalimide based fluorescent photoinduced electron transfer (PET) chemosensors for Zn (II) under physiological pH conditions. Org. Biomol. Chem., 5 (2007), pp. 310–317
[47] H. Mu, R. Gong, Q. Ma, Y. Sun, E. Fu. A novel colorimetric and fluorescent chemosensor: synthesis and selective detection for Cu^{2+} and Hg^{2+}. Tetrahedron Lett., 48 (2007), pp. 5525–5529
[48] L.K. Limbach, Y. Li, R.N. Grass, T.J. Brunner, M.A. Hintermann, M. Muller, D. Gunther, W.J. Stark. Oxide nanoparticle uptake in human lung fibroblasts: effects of particle size, agglomeration, and diffusion at low concentrations. Environ. Sci. Technol., 39 (2005), pp. 9370–9376
[49] Y. Yang, Z. Mao, W. Huang, L. Liu, J. Li, J. Li, Q. Wu. Redox enzyme-mimicking activities of CeO(2) nanostructures: intrinsic influence of exposed facets. Sci. Rep., 6 (2016), p. 35344
[50] D. Jiang, W. Wang, L. Zhang, Y. Zheng, Z. Wang. Insights into the surface-defect dependence of photoreactivity over CeO2 nanocrystals with well-defined crystal facets. ACS Catal., 5 (2015), pp. 4851–4858
[51] H.-X. Mai, L.-D. Sun, Y.-W. Zhang, R. Si, W. Feng, H.-P. Zhang, H.-C. Liu, C.-H. Yan. Shape-selective synthesis and oxygen storage behavior of ceria nanopolyhedra, nanorods, and nanocubes. J. Phys. Chem. B, 109 (2005), pp. 24380–24385
[52] X. Liu, K. Zhou, L. Wang, B. Wang, Y. Li. Oxygen vacancy clusters promoting reducibility and activity of ceria nanorods. J. Am. Chem. Soc., 131 (2009), pp. 3140–3141
[53] S. Das, S. Singh, J.M. Dowding, S. Oommen, A. Kumar, T.X. Sayle, S. Saraf, C.R. Patra, N.E. Vlahakis, D.C. Sayle, W.T. Self, S. Seal. The induction of angiogenesis by cerium oxide nanoparticles through the modulation of oxygen in intracellular environments. Biomaterials, 33 (2012), pp. 7746–7755
[54] V.N. Kouvelis, C. Wang, A. Skrobek, K.M. Pappas, M.A. Typas, T.M. Butt. Assessing the cytotoxic and mutagenic effects of secondary metabolites produced by several fungal biological control agents with the Ames assay and the VITOTOX® test. Mutat. Res. Genet. Toxicol. Environ. Mutagen., 722 (2011), pp. 1–6
[55] M. Hernando, S. De Vettori, M.M. Bueno, A. Fernández-Alba. Toxicity evaluation with Vibrio fischeri test of organic chemicals used in aquaculture. Chemosphere, 68 (2007), pp. 724–730
[56] S.-A. Choi, C.S. Park, O.S. Kwon, H.-K. Giong, J.-S. Lee, T.H. Ha, C.-S. Lee. Structural effects of naphthalimide-based fluorescent sensor for hydrogen sulfide and imaging in live zebrafish. Sci. Rep., 6 (2016)
[57] M. Brana, M. Cacho, A. Gradillas B.D. Pascual-Teresa, A. Ramos, Intercalators as anticancer drugs. Curr. Pharm. Des., 7 (2001) (1745-1780)
[58] C.T. Miller, R. Weragoda, E. Izbicka, B.L. Iverson. The synthesis and screening of 1, 4, 5, 8-naphthalenetetracarboxylic diimide–peptide conjugates

with antibacterial activity. Bioorg. Med. Chem., 9 (2001), pp. 2015–2024
[59] Z. Zheng, A. Omairi-Nasser, X. Li, C. Dong, Y. Lin, R. Haselkorn, J. Zhao. An amidase is required for proper intercellular communication in the filamentous cyanobacterium *Anabaena* sp. PCC 7120. Proc. Natl. Acad. Sci. (2017), p. 201621424
[60] C. Ge, J. Du, L. Zhao, L. Wang, Y. Liu, D. Li, Y. Yang, R. Zhou, Y. Zhao, Z. Chai. Binding of blood proteins to carbon nanotubes reduces cytotoxicity. Proc. Natl. Acad. Sci., 108 (2011), pp. 16968–16973
[61] J. Aguilera-Sigalat, V.F. Pais, A. Doménech-Carbó, U. Pischel, R.E. Galian, J. Pérez-Prieto. Unconventional fluorescence quenching in naphthalimide-capped CdSe/ZnS nanoparticles. J. Phys. Chem. C, 117 (2013), pp. 7365–7375
[62] P. Du, W.-H. Zhu, Y.-Q. Xie, F. Zhao, C.-F. Ku, Y. Cao, C.-P. Chang, H. Tian. Dendron-functionalized macromolecules: enhancing core luminescence and tuning carrier injection. Macromolecules, 37 (2004), pp. 4387–4398
[63] L. Bekere, D. Gachet, V. Lokshin, W. Marine, V. Khodorkovsky. Synthesis and spectroscopic properties of 4-amino-1, 8-naphthalimide derivatives involving the carboxylic group: a new molecular probe for ZnO nanoparticles with unusual fluorescence features. Beilstein J. Org. Chem., 9 (2013), pp. 1311–1318
[64] R. Huang, R.P. Carney, K. Ikuma, F. Stellacci, B.L. Lau. Effects of surface compositional and structural heterogeneity on nanoparticle–protein interactions: different protein configurations. ACS Nano, 8 (2014), pp. 5402–5412
[65] A. Othman, K. Bear, S. Andreescu. Quantitative assay for the detection, screening and reactivity evaluation of nanoceria particles. Talanta, 164 (2017), pp. 668–676
[66] A. Chatterjee, M. Santra, N. Won, S. Kim, J.K. Kim, S.B. Kim, K.H. Ahn. Selective fluorogenic and chromogenic probe for detection of silver ions and silver nanoparticles in aqueous media. J. Am. Chem. Soc., 131 (2009), pp. 2040–2041
[67] P.G. Corrie. Cytotoxic chemotherapy: clinical aspects. Medicine, 36 (2008), pp. 24–28

SUPPLEMENTARY MATERIAL

Physicochemical and biological interactions between cerium oxide nanoparticles and a 1,8-naphthalimide derivative

Gerardo Pulido-Reyesa[1,3,*], Esperanza Martín[2], J.L. Gu. Coronado[2], Francisco Leganes[1], Roberto Rosal[3], Francisca Fernández-Piñas[1]

[1] Departamento de Biología, Facultad de Ciencias, Universidad Autónoma de Madrid, E-28049, Spain
[2] Departamento de Química-Física Aplicada, Facultad de Ciencias, Universidad Autónoma de Madrid, E-28049, Spain
[3] Departamento de Ingeniería Química, Universidad de Alcalá, E-28871 Alcalá de Henares, Madrid, Spain

* Corresponding author: gerardo.pulido@uam.es

Supplementary table S1. Composition of the cyanobacterial growth medium AA/8 [**].

Component	Final concentration (mM)
KH_2SO_4	0.25
$MgSO_4$	0.125
$CaCl_2$	0.0625
NO_3	5
NaCl	0.5
Na_2-EDTA	0.009625
$FeSO_4$	0.08375
B	0.00053125
Co	0.00002125
Cu	0.00004
Mn	0.00093
Mo	0.00015625
Zn	0.000095
V	0.000025

[**] Miguel González-Pleiter, 2013. Toxicity of five antibiotics and their mixtures towards photosynthetic aquatic organisms: Implications for environmental risk assessment. Water Res. 47(6), 2050-2064. 2013.

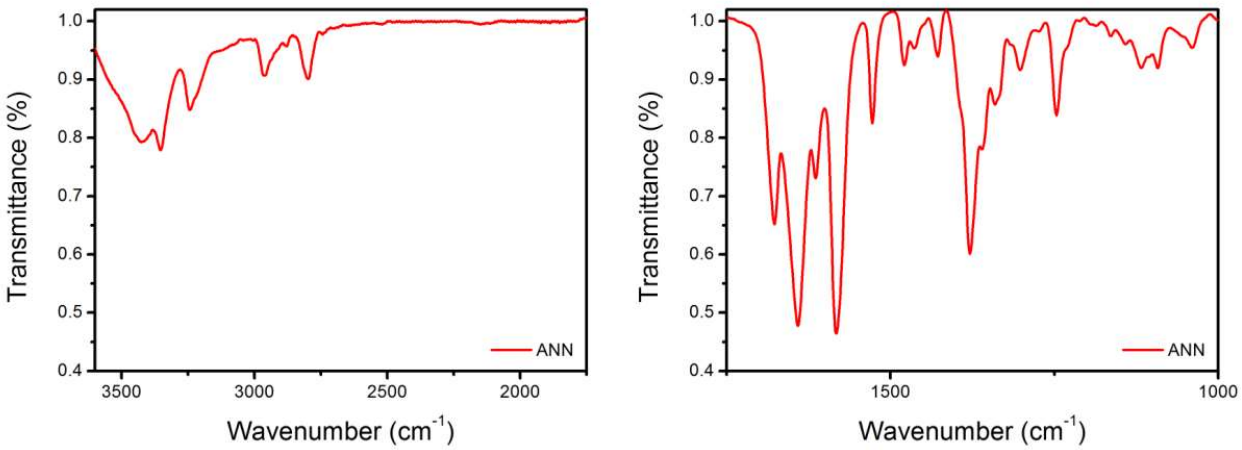

Supplementary Figure S1. FTIR transmission spectrum of ANN in the 3600-1750 cm^{-1} range (left) and 1750-1000 cm^{-1} range (right).

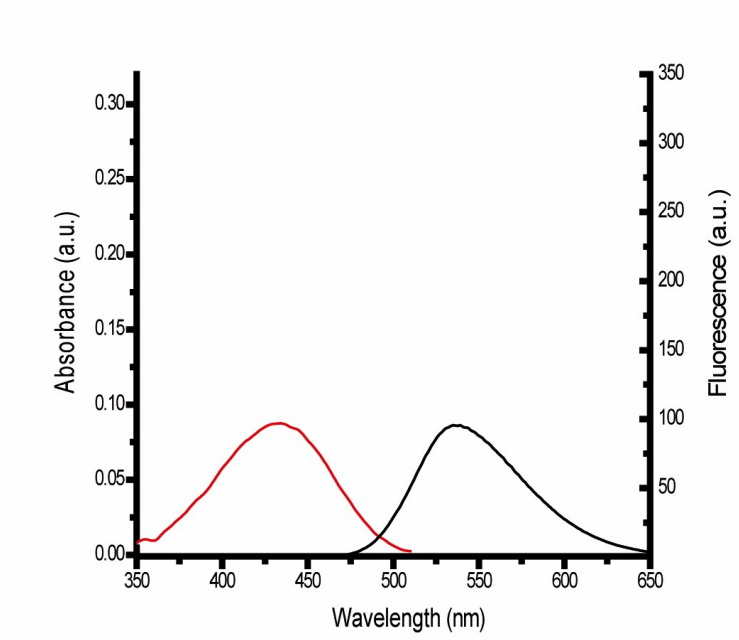

Supplementary Figure S2. The absorption (red line) and emission spectra (black line) of ANN in dH_2O at pH 7.0.

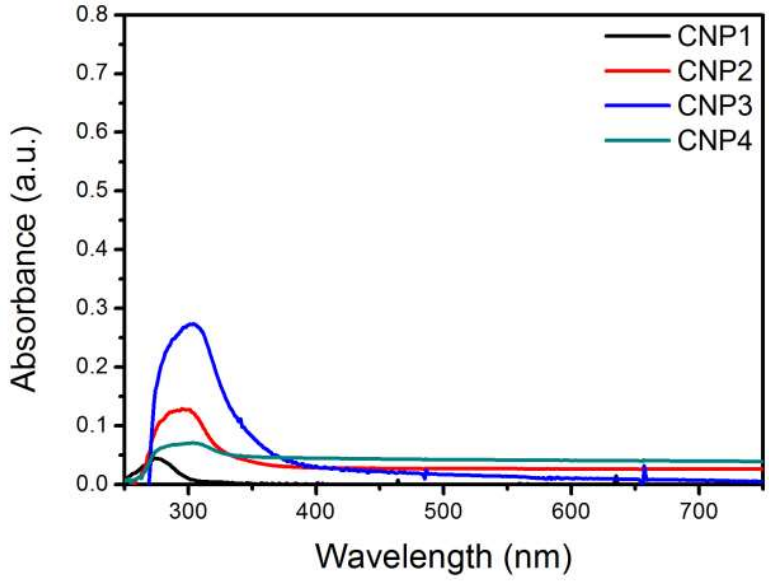

Supplementary Figure S3. The absorption spectra of CNPs in dH_2O from 250 to 750 nm.

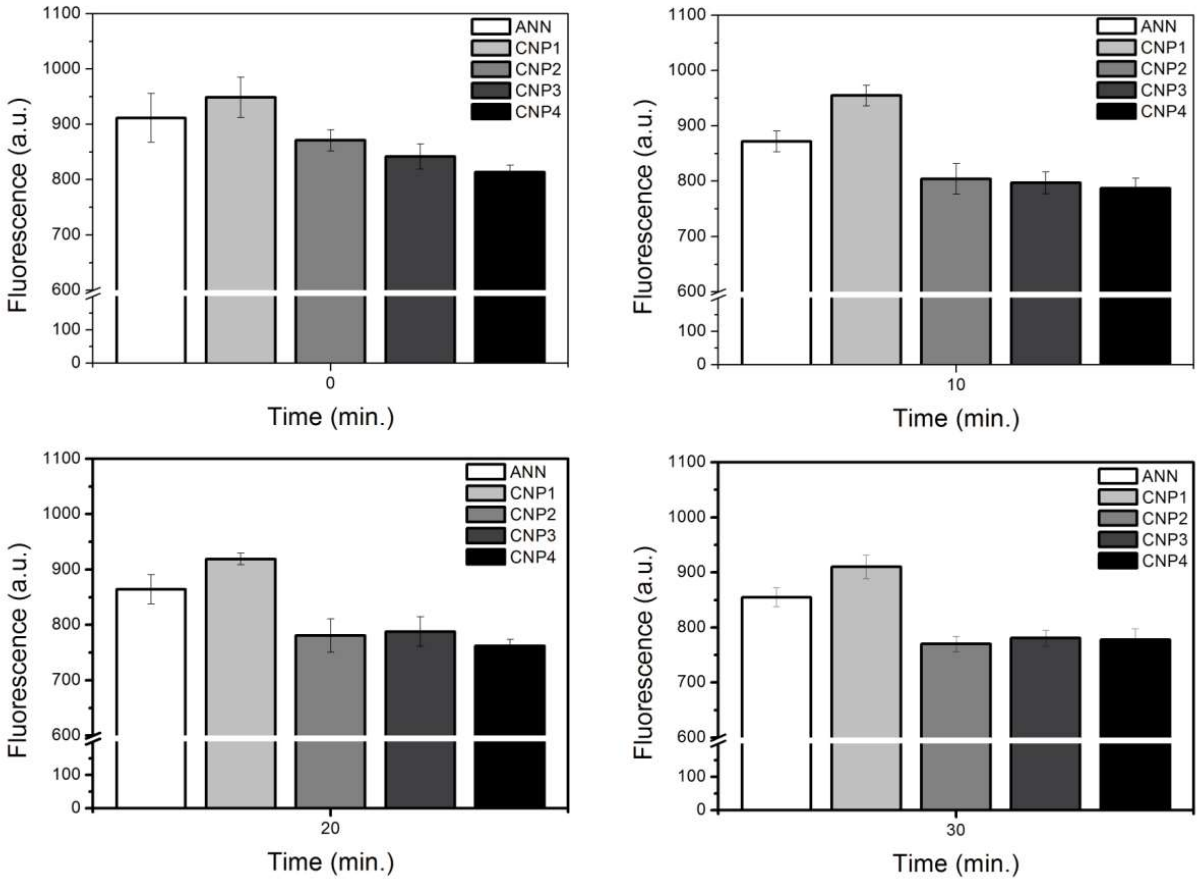

Supplementary Figure S4. Fluorescence emission (Ex/Em 360/560 nm) of ANN and mixtures with CNPs at 1, 10, 20 and 30 min after CNP addition. Mean ± standard deviation.